Journal of Advanced Research (2016) 7, 463–472

Cairo University

Journal of Advanced Research

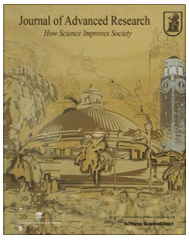

ORIGINAL ARTICLE

Metallurgical and mechanical properties of laser welded high strength low alloy steel

Ramachandran Oyyaravelu *, **Palaniyandi Kuppan, Natarajan Arivazhagan**

School of Mechanical Engineering, VIT University, Vellore 632014, India

GRAPHICAL ABSTRACT

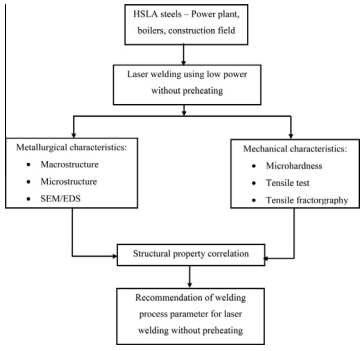

ARTICLE INFO

Article history:
Received 4 January 2016
Received in revised form 14 March 2016
Accepted 15 March 2016
Available online 21 March 2016

Keywords:
Nd:YAG laser welding
HSLA steel

ABSTRACT

The study aimed at investigating the microstructure and mechanical properties of Neodymium-Doped Yttrium Aluminum Garnet (Nd:YAG) laser welded high strength low alloy (HSLA) SA516 grade 70 boiler steel. The weld joint for a 4 mm thick plate was successfully produced using minimum laser power of 2 kW by employing a single pass without any weld preheat treatment. The micrographs revealed the presence of martensite phase in the weld fusion zone which could be due to faster cooling rate of the laser weldment. A good correlation was found between the microstructural features of the weld joints and their mechanical properties. The highest hardness was found to be in the fusion zone of cap region due to formation of martensite and also enrichment of carbon. The hardness results also showed a narrow soft zone at the heat affected zone (HAZ) adjacent to the weld interface, which has no effect on the weld tensile

* Corresponding author. Tel.: +91 9843016937.
E-mail address: royyaravelu@vit.ac.in (R. Oyyaravelu).

Peer review under responsibility of Cairo University.

ELSEVIER Production and hosting by Elsevier

http://dx.doi.org/10.1016/j.jare.2016.03.005

SA516 grade 70
Mechanical properties
Metallurgical properties

strength. The yield strength and ultimate tensile strength of the welded joints were 338 MPa and 549 MPa, respectively, which were higher than the candidate metal. These tensile results suggested that the laser welding process had improved the weld strength even without any weld preheat treatment and also the fractography of the tensile fractured samples showed the ductile mode of failure.

Introduction

Laser beam welding has become one of the important welding techniques used in modern industries because of its superior properties such as high welding speed, low thermal distortion, ease of automation, thin and small weld seams and the possibility of online control of quality during the process [1,2]. Nd:YAG and CO_2 lasers are being widely used in the industries such as ship building, defense and aerospace sectors. Recently, the solid state lasers such as disk laser, diode laser and fiber laser with high wall plug efficiency and superior beam quality have been developed [3–6]. With smaller heat input and higher cooling rate, the laser welding has more advantages compared to the submerged arc welding and the multi-pass gas metal arc welding. Similarly, compared to the friction stir welding and the resistance spot welding, the laser welding becomes more productive because of its automation and flexibility [7].

High strength low alloy (HSLA) steels are being widely used in structural applications because of its high yield strength and good weldability. Typically, HSLA steels have microstructures consisting mainly of ferrite, pearlite, small amount of carbides, carbonitrides and nitrides depending on the heat treatment and processing received during production [8]. The yield and tensile strength of HSLA steels range from 275 to 550 MPa and 380 to 620 MPa, respectively. ASME SA516 grade 70 steel is one of the widely used HSLA steels for service in lower than ambient temperature applications. This steel has high notch toughness and is used in several applications such as boilers, pressure vessels, bridges, wind turbine towers, oil and gas pipelines in which welding is one of the most critical manufacturing processes [9–11].

Amanie et al. [12] have used submerged arc welding (SAW) for joining of 17 mm thick sections of SA516 grade 70 steel to study the effect of welding parameters such as current and welding speed on impact strength, tensile strength, and microstructure. They observed that welding current was the major significant factor for affecting acicular ferrite in the weld metal. Cao et al. [13] examined weldability of HSLA steel of 9.5 mm thick plate using metal inert gas, laser welding and hybrid laser-arc welding techniques. The authors observed that there were improvements in reduction of distortion and porosity in the weldment while employing both laser and hybrid laser techniques as compared to MIG welding technique. However, the researchers noticed the martensitic and bainitic microstructures in the fusion zone that exhibited higher hardness. The laser welding gives a relatively narrow weld and restricted heat affected zone (HAZ) compared to the arc welding and thus minimizes the residual stress and distortion. Parkes et al. [14] investigated the welding of HSLA using fiber laser. The result shows the formation of martensitic structure, due to the fast cooling at fusion zone (FZ). Sharma and Molian [15] employed Yb:YAG disk laser for joining of advanced high strength steels. They observed a slight concavity at the bottom of the joint. Saha et al. [16] studied on microstructure properties correlation in fiber laser welding of HSLA steels. The tensile fracture showed the stretched out dimpled structures. Further, the author also noticed the fine carbide precipitates in the weldment acting as the crack initiation sites which lead to the formation of the micro voids. Teske and Martins [17] have investigated the influence of the shielding gas composition on Gas Metal Arc (GMA) welding of ASTM A516 steel. The author witnessed fewer inclusions in the welds produced with helium mixtures as the shielding gas. It was also observed that the impact resistance of the welds obtained was influenced by the different compositions of gas mixtures.

The review of literature on welding of HSLA steels indicates that GMAW, SAW and laser welding could be the possible welding methods to meet the industrial needs [18]. However, the published data on laser welding of HSLA SA516 grade 70 steel are very limited. In the view of the above, the present work focuses on an autogenous welding of SA516 grade 70 steel using Nd:YAG continuous wave laser with a minimum power. The effect of laser power and welding speed was analyzed to achieve the minimum bead width and maximum penetration depth. Further, the metallurgical and mechanical characteristics of weldment have been studied. The outcomes of the study would be greatly helpful to the power plant industries employing SA516 steel weld joints.

Table 2 Mechanical properties of base metal SA516 grade 70 steel.

Yield strength, MPa	341.00
Ultimate tensile strength, MPa	563.00
% of elongation	30.00
Impact energy, J	5.50

Table 1 Chemical composition (wt%) of base metal SA516 grade 70 steel.

Element	C	Si	Mn	P	S	Cr	Mo	Ni	Cu	Nb	Ti	V	B	N
Observed values	0.222	0.320	1.12	0013	0.007	0.048	0.006	0.012	0.018	0.014	0.002	0.005	0.001	0.006

Table 3 Macrostructure of bead on weld of SA516 grade 70 steel.

Laser power : 1700 W Welding speed: 400 mm/min	Bead width: 4.3 mm Penetration depth: 3.83 mm	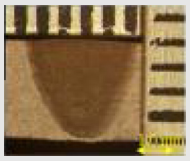
Laser power : 1700 W Welding speed: 500 mm/min	Bead width: 3.95 mm Penetration depth: 3.60 mm	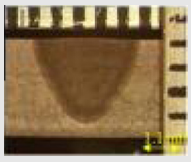
Laser power : 1700 W Welding speed: 600 mm/min	Bead width: 3.6 mm Penetration depth: 3.10 mm	
Laser power : 1850 W Welding speed: 400 mm/min	Bead width: 3.4 mm Penetration depth: 3.9 mm	
Laser power : 1850 W Welding speed: 500 mm/min	Bead width: 3.10 mm Penetration depth: 3.90 mm	
Laser power : 1850 W Welding speed: 600 mm/min	Bead width: 3.3 mm Penetration depth: 3.8 mm	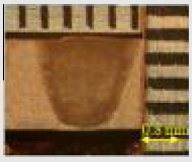
Laser power : 2000 W Welding speed: 400 mm/min	Bead width: 3.6 mm Penetration depth: 4.0 mm	
Laser power : 2000 W Welding speed: 500 mm/min	Bead width: 3.43 mm Penetration depth: 4.0 mm	
Laser power : 2000 W Welding speed: 600 mm/min	Bead width: 3.12 mm Penetration depth: 3.48 mm	

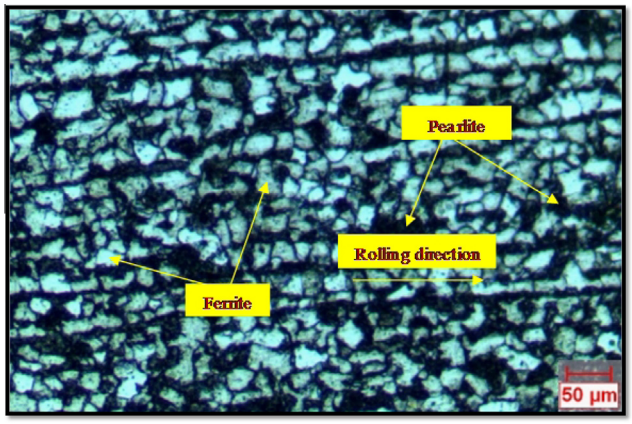

Fig. 1a Microstructure of base metal SA516 grade 70 steel (As received).

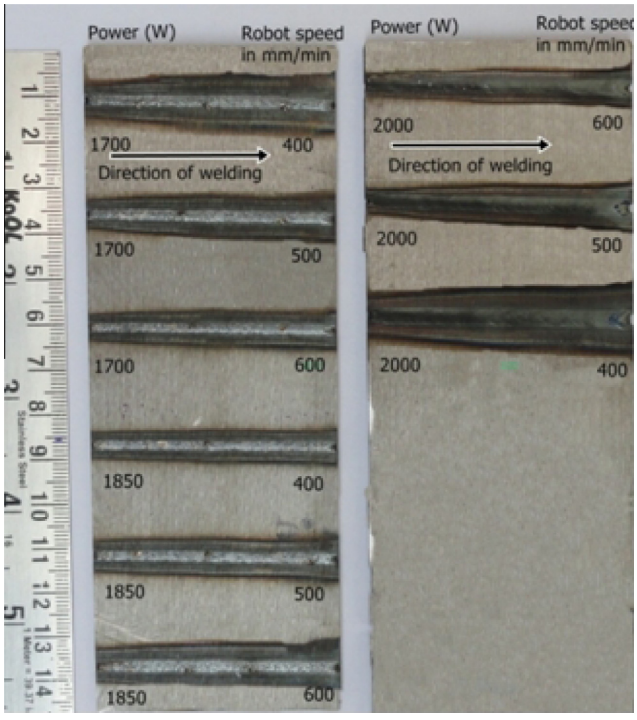

Fig. 1b Photograph of bead on plate of base metal SA516 grade 70 steel.

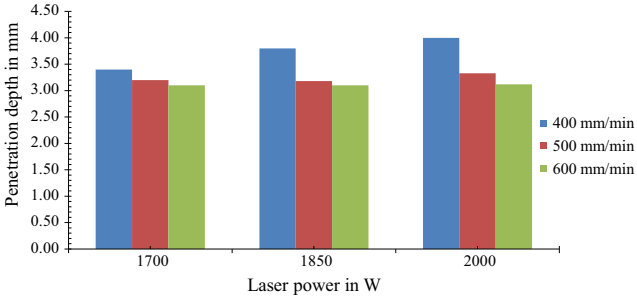

Fig. 1c Penetration depth (mm) vs laser power (W).

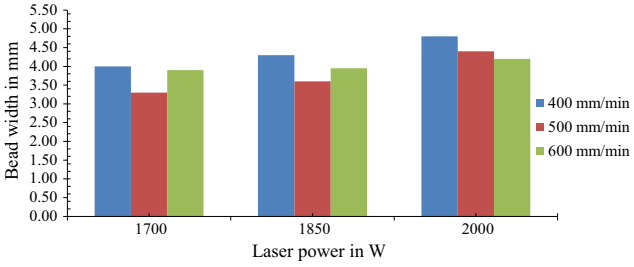

Fig. 1d Bead width (mm) vs laser power (W).

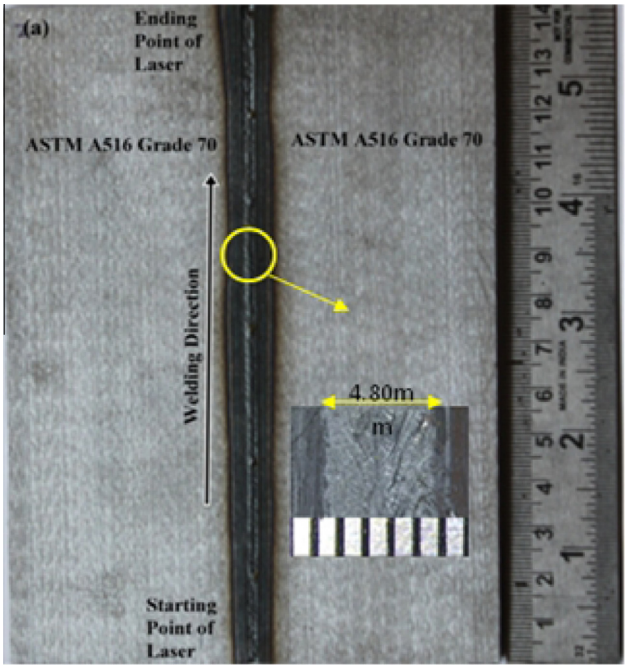

Fig. 2a Photograph of welded sample of SA516 grade 70 steel.

Experimental

The material used for the present experiment was HSLA steel of SA516 grade 70 low-carbon boiler steel and the chemical composition (wt%) of the work material is given in Table 1. The mechanical properties of the candidate metal such as tensile and impact properties are tabulated in Table 2. The candidate metal for the bead on weld study was cut from a plate using wire-EDM process to a size of 120 mm × 60 mm × 4 mm. The top and bottom surfaces were ground to remove the corroded and oxide surfaces and then chemically cleaned with acetone and methanol to eliminate the surface contaminations.

The study of bead on weld was carried out to find out the optimum laser welding parameters for the maximum penetration and minimum bead width. The laser head was tilted about an angle of 5° from the vertical position, in order to avoid the damage due to laser beam back reflection. In addition, the weld pool was protected by argon shielding gas with flow rate of 15 l/min. The welding process parameters were considered over a predetermined range as per the earlier studies [19–23]. The welding process parameters such as laser power and welding speed were taken as variable parameters for this study and

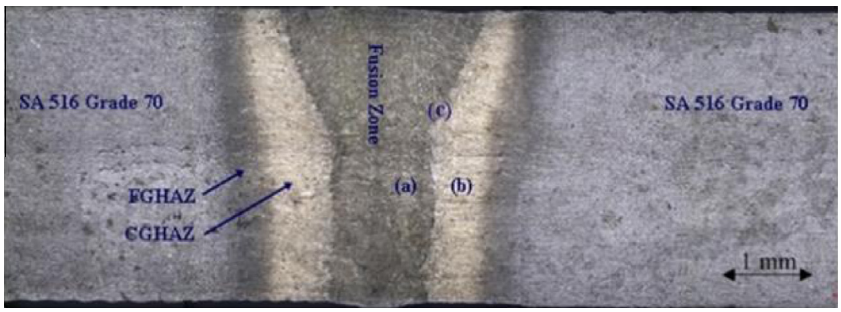

Fig. 2b Macrostructure of the fusion zone, heat affected zone and base metal of welded sample.

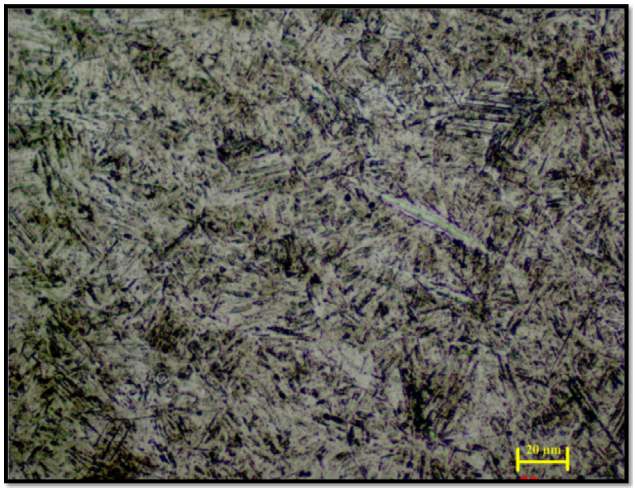

Fig. 3a Microstructure at fusion zone of SA516 grade 70 steel.

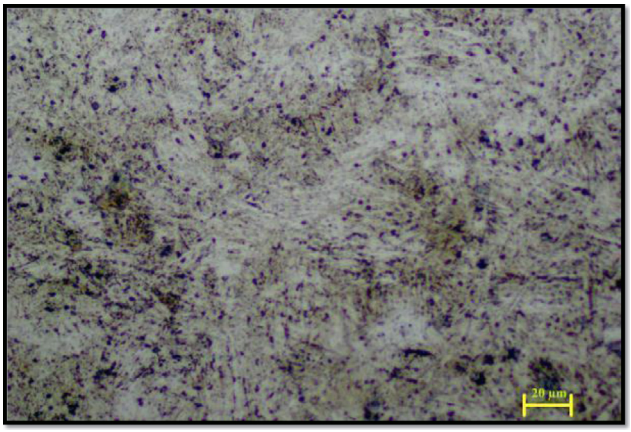

Fig. 3c Microstructure of heat affected zone of SA516 grade 70 steel.

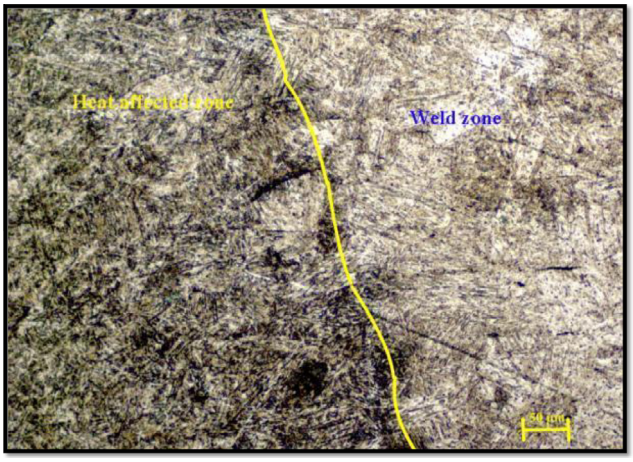

Fig. 3b Microstructure at weld interface of SA516 grade 70 steel.

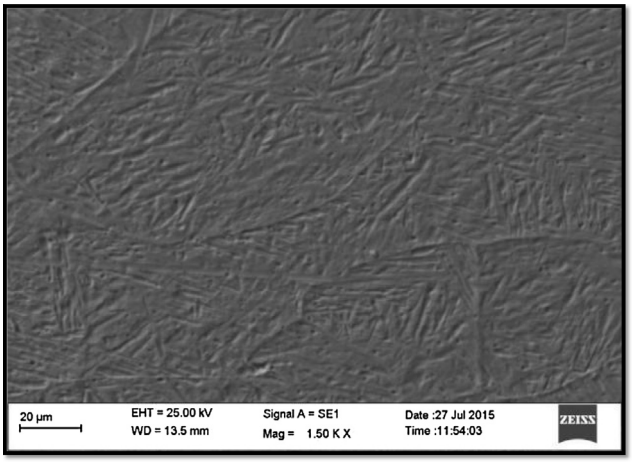

Fig. 4a SEM image at fusion zone of welded joint of SA516 grade 70 steel.

the other parameters such as focusing distance, laser beam mode, and shielding gas flow rate were kept constant. Full factorial experimental design ($3^2 = 9$) was used for the weld bead study experiments. The candidate metal was clamped on a worktable using the strap clamps to avoid the welding distortion. The focal plane was maintained at the top surface of the candidate metal and the focal length of the optics used for the laser delivery was 200 mm. The macro study was carried out by standard metallographic procedure such as mounting, grinding, and polishing using 1 µm diamond suspension followed by etching with 2% Nital solution. The measured experimental results such as weld penetration and bead width were systematically analyzed and the same is shown in Table 3. The optimized welding parameters have been used to produce the square butt joint configuration which is perpendicular to the rolling direction of the candidate metal.

The welded samples were cut across the welding direction and were polished as per the standards and observed using an optical microscope and a scanning electron microscope (SEM), equipped with Oxford energy dispersive X-ray spectroscopy (EDS). Vickers micro-hardness test was performed on the polished samples across the weld for a load of 500 g and a dwell time of 12 s. All indentations were adequately spaced at 0.2 mm to prevent any potential effect of strain fields caused by adjacent indentations.

The tensile test samples were sectioned from the welded coupon in the rolling direction, perpendicular to the welding direction. The tensile tests were carried out by the following ASTM-E8/E8M standard. The samples were sectioned from the welded blanks in such a way that the weld was positioned at the center of the gauge length. The tensile tests were carried out by maintaining a constant cross-head velocity of 2 mm/min to induce a strain rate of $3.3 \times 10^{-4}\ s^{-1}$. Three trials were performed to evaluate the tensile properties of the weldment.

Charpy V-notch impact studies were also carried out on the sub-sized samples (55 mm × 10 mm × 5 mm) obtained as per ASTM: E23-12C standard. The notches were made in weld center in such a way that the failure occurred only within the fusion zones. Further, SEM fractography was carried out on both tensile and impact fractured samples to evaluate the mode of fracture.

Results and discussion

Effect of laser parameters on weld bead width and penetration

The candidate metal selected for this study was designed to have a predominantly ferrite and pearlite structure with finely dispersed alloy carbide particles which is represented in Fig. 1a. The photographs of bead on welds are shown in Fig. 1b. It was noticed from Fig. 1b that the welds produced are free from surface defects. The influence of process parameters such as laser power and welding speed on bead geometry dimensions is shown in Figs. 1c and 1d, respectively. The photograph and cross sectional macrograph of welded sample are shown in Figs. 2a and 2b, respectively. The results revealed that the depth of penetration increases with increasing laser power and decreasing welding speed. The trend observed is in line with the known fact with any welding process that the depth of penetration increases with the increase in heat input. It is observed from the results that full penetration with minimum bead width of 3.6 mm was obtained at a laser power of 2000 W and welding speed of 400 mm/min. The optimum parameters indentified from the bead on weld studies were used to fabricate the weld joints and for further investigations.

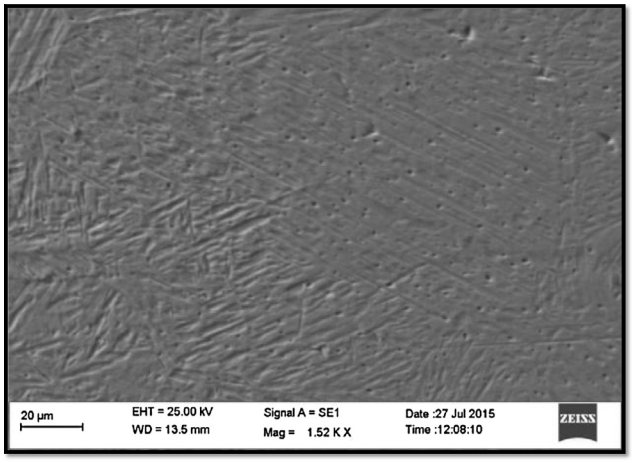

Fig. 4b SEM image at weld interface of welded joint of SA516 grade 70 steel.

Macro and microstructural characterization

The cross-sectional macrograph of the weld joints is shown in Fig. 2b. The weld joint showed proper fusion of base metal and free from any macro level defects. Further, Non-Destructive Testing (NDT) was performed to detect the defects such as under-cuts, porosities, and inclusions as per the ASTM 1417-05 standard.

The detailed micrograph at various locations such as the weld fusion zone, the weld interface and the base metal is shown in Figs. 3a–3c, respectively. In general, the micrograph in the weldment mainly depends on the heat input and the cooling rate. According to continuous cooling transformation diagram of weldment of low carbon steel, micrographs of weld fusion are acicular ferrite, bainite and martensite [24]. However, the micrograph of weld fusion zone was fully martensitic structure along with insignificant amount of bainite. It can be inferred that during the laser welding, the weld zone attained upper critical temperature (AC_3), which favors the austenite formation. It was also inferred that, higher order heat input and rapid cooling rate lead to major transformation of martensite in the weld fusion zone (Fig. 3a). The micrograph of HAZ was found to be martensite along with austenite (co-existence of ferrite and austenite). This can be ascribed that the reduced heat input in HAZ accelerates the cooling and leads to transformation of martensite. In addition, there a few dispersed carbides were also noticed which could be due to enrichment of carbon at the weld and weld interface during the solidification.

The micrograph features of weld fusion zone and weld interface were characterized by SEM/EDS and illustrated in Figs. 4a and 4b. The EDS line mapping analysis demonstrated the absence of elemental variation in the weld zone as well as across the weld interface The SEM line mapping at fusion zone is shown in Fig. 4c. The martensite structure can be seen in the fusion zone. This could be due to the controlled heat input during laser welding. However, in the weld zone with martensitic phase, there was no evidence of hydrogen cracking/weld metal cracking which could be due to consequence of laser welding technique. Further, the absence of segregation in the weld fusion zone would enhance the hot cracking resistance even without any pre-weld heat treatment. It is believed that hot cracking is a contributing factor for the good quality of welds obtained. In this study, it is confined that narrow heat input by laser beam leads to enhanced hot cracking resistance. However, detailed studies are needed to investigate the hot cracking tendency of the weld/HAZ.

Microhardness analysis

The hardness profiles of sample, as measured from the cap, middle and root across the weld are represented in Fig. 5. It was observed that the hardness profile exhibits symmetric

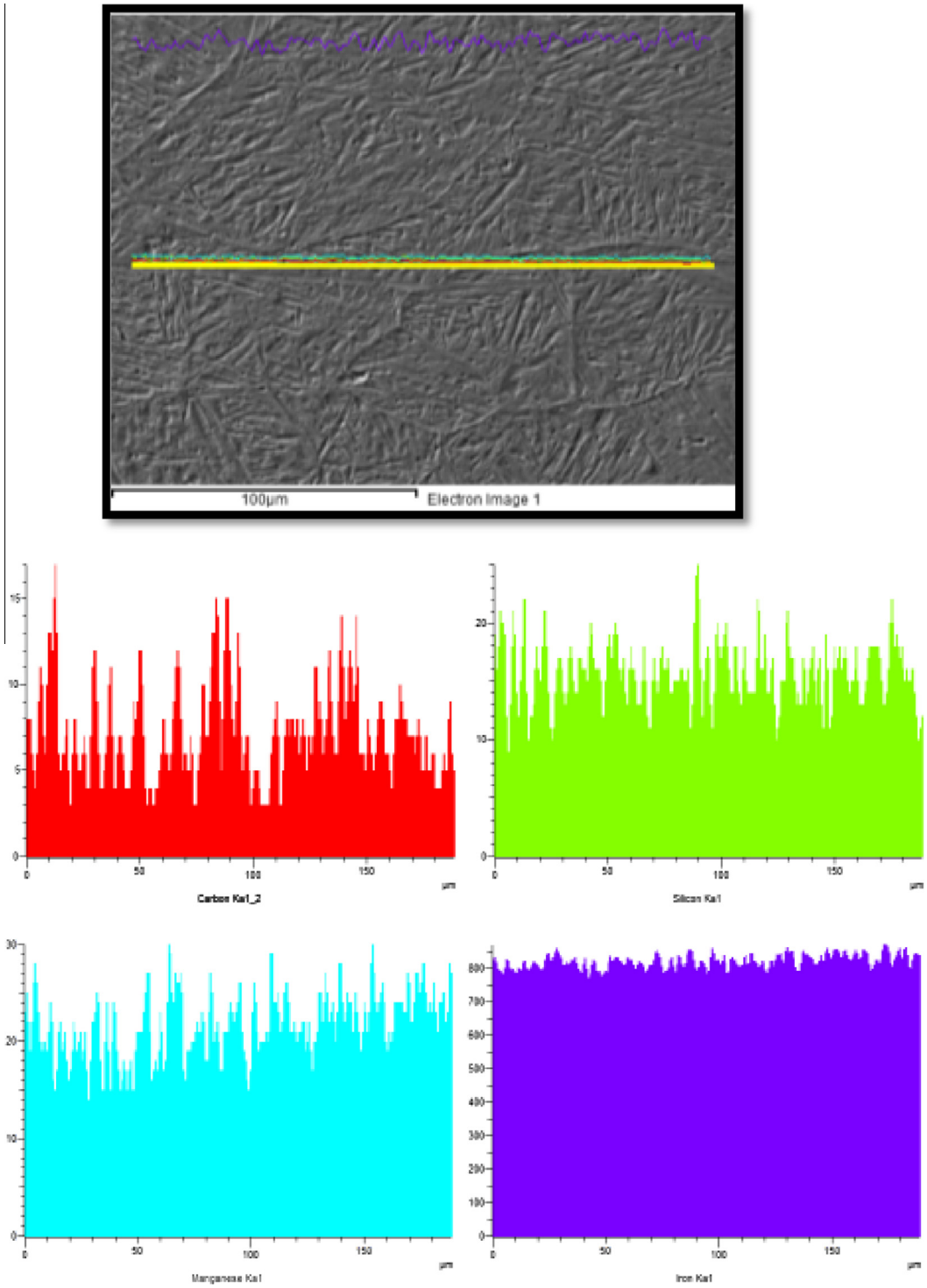

Fig. 4c SEM line mapping at fusion zone of welded joint of SA516 grade 70 steel.

characteristics on both sides of the welded zone. The study shows that the overall hardness in the weld fusion zone increases mainly due to martensite with some carbides. The average hardness of the weld region was 491 HV, whereas the average hardness of the HAZ was 411 HV. The difference of hardness across the weld-HAZ-base metal could be due to changes in metallurgical phase constituents. Hardness measured at the weld fusion zone was nearly 2.5 times that of the candidate material. This could be as a result of the high cooling rate which leads to formation of martensite combined with bainite as reported [25,26]. The variation of hardness in the weld zone also witnessed the formation of martensite as

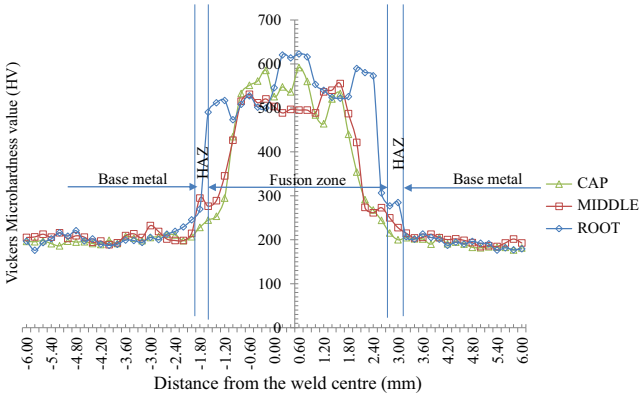

Fig. 5 Microhardness distribution profile of welded joint of SA516 grade 70 steel.

well as formation of bainite structure as a result of chemistry dilution as reported by Saha et al. [16] and Coelho et al. [25].

However, the hardness values in the HAZ were less when compared to the base metal. It should be noted that a soft region appeared in the middle region adjacent to the weld interface. The formation of soft region on the HAZ can be attributed to decarburization which leads to carbon denude zone in which thermal conductivity is relatively low. Moreover, the soft zone observed on the HAZ can also be ascribed to carbon depletion whereas enrichment in the weld zone results leads to formation of hard and brittle carbide phases [7]. However, the results indicated that the presence of narrow soft zone greatly reduced when compared to other welding techniques.

Higher hardness clearly envisaged the formation of martensitic phase and carbides in the weld zone. Further, the fluctuation of hardness at this zone can be attributed to the difference in the carbon content. It is evident from the hardness plots that the hardness at the weld zone and HAZ was found to be greater when compared to other zones of the weldment, suggesting that these zones are strongest part of the joint.

The SEM fractography (Fig. 6b) inferred predominant cleavage fracture features which suggests that inter-diffusion of elements leads to the creation of low ductile quasi cleavage fracture. Similar observation has been made by Wang et al. [27]. The results of hardness well opined with micrograph as well as SEM/EDS results.

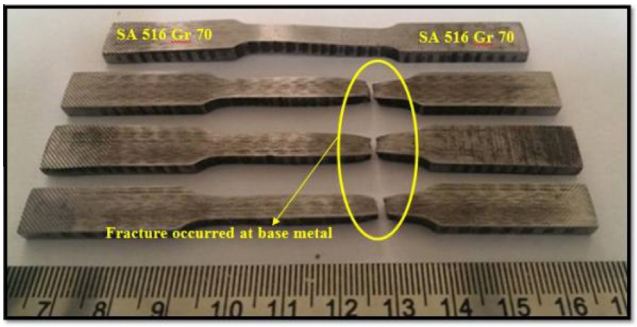

Fig. 6a ASTM E8 standard tensile of laser welded samples with base metal.

Tensile and impact strength analysis

Table 4 shows the tensile and impact properties of laser welded coupons. In order to study the reproducibility of laser welding process, three samples were tested for mechanical properties at the selected welding parameters (Laser power of 2000 W and welding speed of 400 mm/min). Table 4 also shows the reproducibility analysis of tensile and impact properties. The percentage deviation reported for each parameter indicates the variability of parameter with reference to the mean value. The result showed that all the parameters were reproduced within the range of ±6%.

Fig. 6a shows the photograph of tensile fractured samples of weldments. The tensile studies showed that the fracture was encountered in the base metal in all the trials. This indicates that the weld region is comparatively stronger than other regions of the weldment. A necking phenomenon was observed in all the three samples tested with confirmed ductile fracture. Both yield and ultimate tensile strengths of the laser beam welded joints were almost equivalent to the base metal. It is apparent that the soft HAZ and high hardness of the weld fusion zone, results in greater yield strength than the base metal. Compared to the base metal, the elongation to failure is reduced (9%) in all the weld coupons. Further, the tensile results corroborated that the fracture occurred at the parent metal and clearly inferred that the weld strength was greater than the parent metal.

The tensile results can be directly correlated with the hardness data and microstructure. The formation of martensite in the weld zone and HAZ contributed for better strength and hardness. The fracture formation was not experienced in these zones. As the candidate metal offers lower hardness, the tensile

Table 4 Mechanical properties of laser welded joints – reproducibility analysis.

Trail no.	Yield strength (MPa)		Ultimate tensile strength (MPa)		% of elongation		Impact energy, J	
	Expt.	% deviation	Expt.	% deviation	Expt.	% deviation	Expt.	% deviation
1	342.30	1.24	541	−1.46	21.99	3.78	5.1	−0.58
2	319.90	−5.65	551	0.36	20.72	−2.22	5.0	−2.53
3	352.14	4.14	555	1.09	20.39	−3.78	5.3	3.31
Mean	338.11	–	549	–	21.03	–	5.13	–
Std. dev.	16.52	–	7.21	–	1.13	–	0.15	–

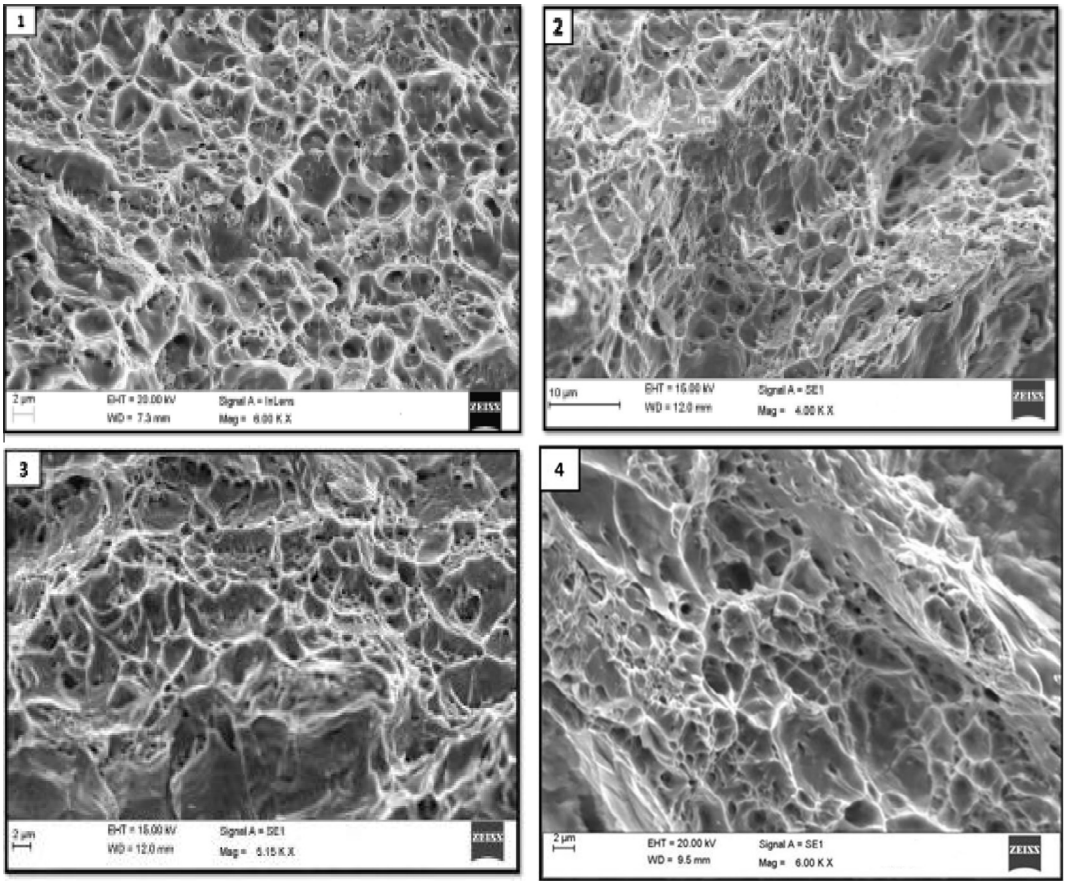

Fig. 6b SEM fractography of the tensile tested SA516 grade 70 steel samples (1 – base metal; 2–4 welded samples).

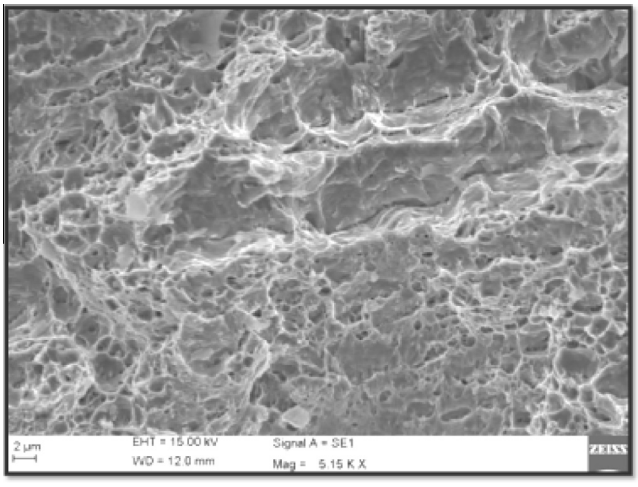

Fig. 6c SEM fractography of an impact tested SA516 grade 70 steel sample.

fracture was experienced at this zone. Further, SEM fractography results divulged the presence of small voids and dimples, which acquainted for a ductile mode of fracture. The SEM fractography of all the three tensile samples and the base metal is shown in Fig. 6b (1 – base metal; 2–4 welded samples).

Further, the Charpy V-notch impact results showed that the impact toughness was found to be lower (5.13 J, average of three samples) than the parent metals (5.5 J) employed in the study. This could be due to the existing high carbon martensite in the fusion zone. It is also inferred from the hardness results that the higher hardness in the weld fusion zone resulted in lower toughness. Further SEM fractography was carried out to investigate the mode of rupture. The absence of fibrous and dimple network along with presence of cleavage facets with deep voids suggests that the mode of failure is brittle. The SEM fractography for the impact test sample is shown in Fig. 6c.

Thus, this study established the weldability, microstructure and mechanical properties of the weld joints of SA516 high strength low alloy steel of 4 mm thick plate. The micrographs obtained by SEM/EDS techniques were used to investigate the metallurgical properties. In addition, mechanical characterization of the weld joint was established by accompanying various tests. Based on the outcomes of the structure–property correlation, it can be concluded that minimum laser power can be used for fabricating weldments of SA516 HSLA steel, without any weld defects such as cold cracking and hydrogen induced cracking. Hence laser welding is recommended for adoption in the power plant industry.

Conclusions

In this investigation, an attempt was made to study the effect of laser welding process by evaluating the metallurgical and

mechanical properties of SA516 grade 70 high strength low alloy steel joints without any weld preheat treatment. The following conclusions are derived from the experimental results:

a. Nd:YAG CW laser produced good quality weldment without any defect such as distortion, cold cracking and hydrogen induced cracking.
b. The weld fusion zone contains martensitic structure due to very high cooling rates associated with laser welding.
c. The microhardness of the fusion zone was found to be approximately 2.5 times the base metal in the welded region, whereas, a narrow soft zone of HAZ was observed near the weld interface.
d. The joint fabricated by laser welding process exhibited higher strength values, and the enhancement in strength value is approximately 13% even without any weld preheat treatment.
e. The tensile failure occurred in the base metal region during the tensile tests for all the trials. The ultimate tensile strength and percent elongation obtained for Nd:YAG CW laser welding are 550 MPa and 9% respectively. The SEM fractography of the tensile samples showed ductile mode of failure.
f. The weld impact strength (5.13 J) was found to be less as compared to base metal (5.5 J) and it is inversely proportional to the hardness.

Conflict of Interest

The authors have declared no conflict of interest.

Compliance with Ethics Requirements

This article does not contain any studies with human or animal subjects.

Acknowledgments

The authors are grateful to the DST-FIST and VIT University for providing the laser welding and Instron servo UTM facility for this research work.

References

[1] Dawes C. Laser welding: a practical guide. Woodhead Publishing; 1992.
[2] Sun Z, Ion JC. Laser welding of dissimilar metal combinations. J Mater Sci 1995;30:4205–14.
[3] Farabi N, Chen DL, Zhou Y. Microstructure and mechanical properties of laser welded dissimilar DP600/DP980 dual-phase steel joints. J Alloys Compd 2011;509:982–9.
[4] You D, Gao X, Katayama S. Multiple-optics sensing of high-brightness disk laser welding process. NDT E Int 2013;60:32–9.
[5] Li J, Nayak SS, Biro E, Panda SK, Goodwin F, Zhou Y. Effects of weld line position and geometry on the formability of laser welded high strength low alloy and dual-phase steel blanks. Mater Des 2013;52:757–66.
[6] Onoro J, Ranninger C. Fatigue behaviour of laser welds of high-strength low-alloy steels. J Mater Process Technol 1997;68:68–70.
[7] Xu W, Westerbaan D, Nayak SSS, Chen DLL, Goodwin F, Biro E, et al. Microstructure and fatigue performance of single and multiple linear fiber laser welded DP980 dual-phase steel. Mater Sci Eng A 2012;553:51–8.
[8] Shenghai Z, Yifu S, Huijuan Q. The technology and welding joint properties of hybrid laser-tig welding on thick plate. Opt Laser Technol 2013;48:381–8.
[9] Seifert H-P, Hickling J, Lister D. 5.06 – corrosion and environmentally-assisted cracking of carbon and low-alloy steels. In: Konings RJM, editor. Compr Nucl Mater. Oxford: Elsevier; 2012. p. 105–42.
[10] Standard A. E8M-04. Stand Test Methods Tens Test Met Mater West Conshohocken ASTM Int; 2004.
[11] Stewart M, Lewis OT. 4 – Mechanical design of pressure vessels. In: Stewart M, Lewis OT, editors. Press Vessel F Man. Gulf Professional Publishing; 2013. p. 133–216.
[12] Amanie J, Oguocha INA, Yannacopoulos S. Effect of submerged arc welding parameters on microstructure of SA516 steel weld metal. Can Metall Q 2012;51:48–57.
[13] Cao X, Wanjara P, Huang J, Munro C, Nolting A. Hybrid fiber laser – Arc welding of thick section high strength low alloy steel. Mater Des 2011;32:3399–413.
[14] Parkes D, Xu W, Westerbaan D, Nayak SS, Zhou Y, Goodwin F, et al. Microstructure and fatigue properties of fiber laser welded dissimilar joints between high strength low alloy and dual-phase steels. Mater Des 2013;51:665–75.
[15] Sharma RS, Molian P. Weldability of advanced high strength steels using an Yb:YAG disk laser. J Mater Process Technol 2011;211:1888–97.
[16] Saha DCC, Westerbaan D, Nayak SSS, Biro E, Gerlich APP, Zhou Y. Microstructure-properties correlation in fiber laser welding of dual-phase and HSLA steels. Mater Sci Eng A 2014;607:445–53.
[17] Teske M, Martins F. The influence of the shielding gas composition on GMA welding of ASTM A 516 steel. Weld Int 2010;24:222–30.
[18] Majumdar JD, Manna I. Laser-assisted fabrication of materials, vol. 161. Springer Science & Business Media; 2012.
[19] Sathiya P, Abdul Jaleel MY. Measurement of the bead profile and microstructural characterization of a CO_2 laser welded AISI 904 L super austenitic stainless steel. Opt Laser Technol 2010;42:960–8.
[20] Yang D, Li X, He D, Nie Z, Huang H. Optimization of weld bead geometry in laser welding with filler wire process using Taguchi's approach. Opt Laser Technol 2012;44:2020–5.
[21] Zhang C, Song X, Lu P, Hu X. Effect of microstructure on mechanical properties in weld-repaired high strength low alloy steel. Mater Des 2012;36:233–42.
[22] Koilraj M, Sundareswaran V, Vijayan S, Koteswara Rao SR. Friction stir welding of dissimilar aluminum alloys AA2219 to AA5083 – Optimization of process parameters using Taguchi technique. Mater Des 2012;42:1–7.
[23] Carlone P, Palazzo GS. Influence of process parameters on microstructure and mechanical properties in AA2024-T3 friction stir welding. Metallogr Microstruct Anal 2013;2:213–22.
[24] Kou S. Welding metallurgy. Cambridge Univ Press; 1987.
[25] Coelho RS, Corpas M, Moreto JA, Jahn A, Standfuß J, Kaysser-Pyzalla A, et al. Induction-assisted laser beam welding of a thermomechanically rolled HSLA S500MC steel: a microstructure and residual stress assessment. Mater Sci Eng A 2013;578:125–33.
[26] Guo W, Crowther D, Francis JA, Thompson A, Liu Z, Li L. Microstructure and mechanical properties of laser welded S960 high strength steel. Mater Des 2015;85:534–48.
[27] Wang C, Wang M, Shi J, Hui W, Dong H. Effect of microstructural refinement on the toughness of low carbon martensitic steel. Scr Mater 2008;58:492–5.